



Cite this: RSC Adv., 2018, 8, 29513

# Experimental and theoretical interpretation of the magnetic behavior of two Dy(III) single-ion magnets constructed through $\beta$ -diketonate ligands with different substituent groups ( $-\text{Cl}/-\text{OCH}_3$ )<sup>†</sup>

Sheng Zhang, <sup>\*ac</sup> Wenjiao Mo,<sup>a</sup> Jiangwei Zhang, <sup>d</sup> Haipeng Wu,<sup>b</sup> Min Li,<sup>b</sup> Xingqiang Lü, <sup>c</sup> Bing Yin <sup>\*b</sup> and Desuo Yang<sup>\*a</sup>

Two Dy(III) single-ion magnets, formulated as  $[\text{Dy}(\text{Phen})(\text{Cl}-\text{tcpb})_3]$  (Cl-1) and  $[\text{Dy}(\text{Phen})(\text{CH}_3\text{O}-\text{tmpd})_3]$  ( $\text{CH}_3\text{O}-2$ ) were obtained through  $\beta$ -diketonate ligands ( $\text{Cl}-\text{tcpb} = 1\text{-}(4\text{-chlorophenyl})\text{-}4,4,4\text{-trifluoro-}1,3\text{-butanedione}$  and  $\text{CH}_3\text{O}-\text{tmpd} = 4,4,4\text{-trifluoro-}1\text{-}(4\text{-methoxyphenyl})\text{-}1,3\text{-butanedione}$ ) with different substituent groups ( $-\text{Cl}/-\text{OCH}_3$ ) and auxiliary ligand, 1,10-phenanthroline (Phen). The Dy(III) ions in Cl-1 and  $\text{CH}_3\text{O}-2$  are eight-coordinate, with an approximately square antiprismatic (SAP,  $D_{4d}$ ) and trigonal dodecahedron ( $D_{2d}$ )  $\text{N}_2\text{O}_6$  coordination environment, respectively, in the first coordination sphere. Under zero direct-current (dc) field, magnetic investigations demonstrate that both Cl-1 and  $\text{CH}_3\text{O}-2$  display dynamic magnetic relaxation of single-molecule magnet (SMM) behavior with different effective barriers ( $U_{\text{eff}}$ ) of  $105.4\text{ cm}^{-1}$  (151.1 K) for Cl-1 and  $132.5\text{ cm}^{-1}$  (190.7 K) for  $\text{CH}_3\text{O}-2$ , respectively. As noted, compound  $\text{CH}_3\text{O}-2$  possesses a higher effective barrier than Cl-1. From *ab initio* calculations, the energies of the first excited state ( $\text{KD}_1$ ) are indeed close to the experimental  $U_{\text{eff}}$  as  $126.7\text{ cm}^{-1}$  vs.  $105.4\text{ cm}^{-1}$  for Cl-1 and  $152.8\text{ cm}^{-1}$  vs.  $132.5\text{ cm}^{-1}$  for  $\text{CH}_3\text{O}-2$ . The order of the calculated energies of  $\text{KD}_1$  is same as that of the experimental  $U_{\text{eff}}$ . The superior SMM properties of  $\text{CH}_3\text{O}-2$  could have originated from the larger axial electrostatic potential ( $\text{ESP}_{(\text{ax})}$ ) felt by the central Dy(III) ion when compared with Cl-1. The larger  $\text{ESP}_{(\text{ax})}$  of  $\text{CH}_3\text{O}-2$  arises from synergic effects of the more negative charge and shorter Dy–O distances of the axial O atoms of the first sphere. These charges and distances could be influenced by functional groups outside the first sphere, e.g.,  $-\text{Cl}$  and  $-\text{OCH}_3$ .

Received 23rd July 2018  
 Accepted 6th August 2018

DOI: 10.1039/c8ra06240d  
[rsc.li/rsc-advances](http://rsc.li/rsc-advances)

## 1. Introduction

Since the first single-molecule magnet (SMM),  $\text{Mn}_{12}\text{Ac}$ , was discovered in the 1990s,<sup>1</sup> the search for improved properties, in particular the enhanced relaxation barrier ( $U_{\text{eff}}$ ) and blocking temperature ( $T_B$ ), has advanced the development of new compounds with magnetic properties customized by the coordination environment.<sup>2</sup> The relevant explorations focus on mononuclear lanthanide compounds, especially single Dy-

center systems, owing to the intrinsic strong spin-orbit coupling and large magnetic anisotropy of lanthanide ions.<sup>3</sup> Furthermore, the relatively simple structure is convenient for chemists to improve the understanding of the magneto-structural correlation by combining with *ab initio* calculations.<sup>4</sup> The number of mononuclear lanthanide SMMs or single-ion magnets (SIMs) derived from the above approach, following significantly slow relaxations of the magnetization, has grown significantly. An equatorially coordinated triangular geometry for  $C_3$ ,<sup>5</sup> square antiprismatic systems for  $D_{4d}$ ,<sup>6</sup> sandwich-type systems for  $D_{8d}$  or  $D_{8h}$ ,<sup>7</sup> the pentagonal bipyramidal local geometry for  $D_{5h}$ ,<sup>4a,4b,8</sup> linear 2-coordinated systems for  $D_{\infty h}$ ,<sup>9</sup> and some systems possessing high charge distribution symmetry,<sup>10</sup> are given different priorities in lanthanide SIM construction. The research reveals that the single-ion magnetic anisotropy of lanthanide ions is extremely sensitive to the subtle changes in the ligand and the local geometrical symmetry. The electrostatic potential distribution around the magnetic center can be regulated by the amount of solvent,<sup>11</sup> the anion ligands,<sup>12</sup> the lattice/coordinated solvents,<sup>13</sup> the pH values of the solution systems,<sup>14</sup> or the counter ions,<sup>15</sup> on the basis of weakening or

<sup>a</sup>College of Chemistry and Chemical Engineering, Baoji University of Arts and Sciences, Baoji 721013, China. E-mail: zhangsheng19890501@163.com; yangdesuo@163.com

<sup>b</sup>Key Laboratory of Synthetic and Natural Functional Molecule Chemistry of Ministry of Education, College of Chemistry and Materials Science, Northwest University, Xi'an, Shaanxi 710069, China. E-mail: rayinyin@nwu.edu.cn

<sup>c</sup>School of Chemical Engineering, Shaanxi Key Laboratory of Degradable Medical Material, Northwest University, Xi'an 710069, Shaanxi, China

<sup>d</sup>State Key Laboratory of Catalysis & Gold Catalysis Research Center, Dalian Institute of Chemical Physics, Chinese Academy of Sciences (CAS), China

<sup>†</sup> Electronic supplementary information (ESI) available. CCDC 1815605 and 1815606. For ESI and crystallographic data in CIF or other electronic format see DOI: 10.1039/c8ra06240d

strengthening the electron density.<sup>16</sup> Interestingly, other functional groups from ligands outside the first sphere could also effectively influence the electron density of the first-sphere atoms and thus affect the SIM properties, which should also be considered in the rational design of promising molecular magnets.<sup>4d</sup>

Finding a feasible strategy to regulate and control the electrostatic environment around the metal centers and the single-ion magnetic anisotropy in SIMs would provide an active direction for understanding the magneto-structural correlation in depth and developing magnetic materials with high  $U_{\text{eff}}$  and blocking temperature ( $T_B$ ). Herein, two  $\beta$ -diketonate ligands with different functional groups were chosen for the following reasons: the classical  $\beta$ -diketonate ligands with different functional groups usually coordinate with metal ions in bidentate chelating modes in SIMs, which is beneficial for discussing the influence of the electron density.<sup>8</sup> Fortunately, with the introduction of a capping ligand, two mononuclear compounds,  $[\text{Dy}(\text{Phen})(\text{Cl-tcpb})_3]$  (Phen = 1,10-phenanthroline, Cl-tcpb = 1-(4-chlorophenyl)-4,4,4-trifluoro-1,3-butanedione, **Cl-1**) and  $[\text{Dy}(\text{Phen})(\text{CH}_3\text{O-tmpd})_3]$  ( $\text{CH}_3\text{O-tmpd}$  = 4,4,4-trifluoro-1-(4-methoxyphenyl)-1,3-butanedione, **CH<sub>3</sub>O-2**), were obtained through solution reaction. The Dy(III) ion in compound **Cl-1** has an approximately square antiprismatic (SAP)  $\text{N}_2\text{O}_6$  coordination environment, while **CH<sub>3</sub>O-2** has a trigonal dodecahedron ( $D_{2d}$ ) configuration. Magnetic characterization indicates that the subtle changes in the different substituent groups from the  $\beta$ -diketonate ligand results in great differences in the coordination environment and dramatically alters the relaxation behaviors of **Cl-1** and **CH<sub>3</sub>O-2**. To further understand the different magnetic behaviors of **Cl-1** and **CH<sub>3</sub>O-2**, *ab initio* calculations were also performed to explore the magnetic anisotropies of the central Dy(III) ions. A preliminary analysis on the electrostatic potential felt by the Dy(III) ion is utilized to identify the effect of ligands on its magnetic anisotropy. Expectedly, other functional groups outside the first sphere could also effectively influence the electron density of the first sphere atoms and thus affect the SIM properties.

## 2. Experimental

### 2.1 Materials and instruction

All the materials and reagents were obtained commercially without further purification. The FT-IR spectra were recorded in the range of 400–4000  $\text{cm}^{-1}$  using KBr pellets on an EQUINOX55 FT/IR spectrophotometer. Elemental analysis (C, H, N) was implemented on a Perkin-Elmer 2400 CHN elemental analyzer. The phase purity of the bulk or polycrystalline samples were confirmed by powder X-ray diffraction (PXRD) measurements executed on a Rigaku RU200 diffractometer at 60 kV, 300 mA, and Cu  $\text{K}\alpha$  radiation ( $\lambda = 1.5406 \text{ \AA}$ ), with a scan speed of 5°  $\text{min}^{-1}$  and a step size of 0.02° in  $2\theta$ . Diffuse reflectance spectra were obtained by a U-41000 spectrophotometer applying  $\text{BaSO}_4$  powder as a 100% reflectance reference. Magnetic measurements were performed in the temperature range of 1.8–300 K with an applied field of 1000 Oe, using a Quantum Design MPMS-XL-7 SQUID magnetometer on polycrystalline samples.

The diamagnetic corrections for the compounds were estimated using Pascal's constants. Alternating current (ac) susceptibility experiments were performed using an oscillating ac field of 2.0 Oe at ac frequencies ranging from 1 to 1000 Hz. The magnetization was measured in the field range 0–7 T.

### 2.2 Synthesis and characterization of the lanthanide compounds

All chemicals were obtained from commercial sources and were used as received without further purification.

**Synthesis of  $[\text{Dy}(\text{Phen})(\text{Cl-tcpb})_3]$  (Cl-1).** A methanol solution (10 mL) of  $\text{Dy}(\text{NO}_3)_3 \cdot 6\text{H}_2\text{O}$  (0.1 mmol, 0.0456 g) and Phen (0.1 mmol, 0.0200 g) was added to a solution of Cl-tcpb (0.3 mmol, 0.0753 g) and KOH (0.3 mmol, 0.0168 g) in 10 mL of dichloromethane under stirring. The resultant solution was filtered and allowed to stand undisturbed at room temperature for three weeks. Block crystals of **Cl-1** were obtained in 37% yield (based on the Dy(III) salt). Anal. Calcd for  $\text{C}_{45}\text{H}_{32}\text{DyF}_9\text{N}_2\text{O}_6$ : C, 52.42; H, 3.11; N, 2.72. Found: C, 52.77; H, 3.32; N, 2.53. IR (KBr): 3077 (w), 1645 (s), 1623 (m), 1553 (s), 1564 (m), 1453 (w), 1401 (m), 1334 (w), 1299 (s), 1168 (m), 1111 (s), 1043 (w), 1009 (m), 923 (m), 833 (m), 801 (w), 775 (w), 722 (w), 677 (w), 611 (m), 575 (w), 487 (m), 439  $\text{cm}^{-1}$ .

**Synthesis of  $[\text{Dy}(\text{Phen})(\text{CH}_3\text{O-tmpd})_3]$  (CH<sub>3</sub>O-2).** A similar synthetic procedure to that for **Cl-1** was used to synthesize **CH<sub>3</sub>O-2**, except that Cl-tcpb (0.3 mmol, 0.0753 g) was replaced by CH<sub>3</sub>O-tmpd (0.3 mmol, 0.0738 g). Finally, pink block crystals were obtained after three weeks in 51% yield (based on the Dy(III) salt). Anal. Calcd for  $\text{C}_{47}\text{H}_{36}\text{DyF}_9\text{N}_2\text{O}_7$ : C, 52.50; H, 3.35; N, 2.61. Found: C, 52.38; H, 3.52; N, 2.82. IR (KBr): 3092 (w), 1621 (s), 1589 (s), 1567 (s), 1533 (s), 1462 (m), 1401 (m), 1343 (w), 1302 (m), 1166 (m), 1145 (m), 1054 (w), 1022 (m), 921 (w), 846 (m), 766 (m), 755 (w), 732 (w), 681 (m), 587 (m), 572 (m), 481 (w), 443 (w), 409 (m)  $\text{cm}^{-1}$ .

### 2.3 X-ray single-crystal diffraction analysis

The single crystal X-ray experiment was performed on an Agilent Xcalibur Eos Gemini diffractometer using graphite-monochromatized Cu  $\text{K}\alpha$  radiation ( $\lambda = 1.5418 \text{ \AA}$ ). The data integration and reduction were processed with the CrysAlisPro software. Absorption correction based on multi-scans was performed using the SADABS program.<sup>17</sup> The structures were solved by the direct method and refined by means of full-matrix least-squares procedures on  $F^2$  with the SHELXL program.<sup>18</sup> All non-hydrogen atoms were refined anisotropically. Other details of crystal data, data collection parameters, and refinement statistics are given in Table S1.† The selected bond lengths and angles are listed in Table S2.†

### 2.4 Theoretical methods and computational details

Multiconfigurational *ab initio* calculations, including spin-orbit coupling (SOC), were performed on the experimental structures of **1** and **2** to explore their magnetic anisotropy. This type of calculation includes two steps:<sup>19</sup> (1) a set of spin eigenstates, were obtained by the state-averaged (SA) CASSCF method;<sup>20</sup> (2) the low-lying SOC states, *i.e.*, Kramers doublets



(KD) herein, were obtained by state interaction, which is the diagonalization of the SOC matrix in the space spanned by the spin eigenstates from the first step. In the CASSCF step, the active space consisted of 9 electrons in 7 orbitals and all the spin eigenstates of 21 sextets were included. Due to the hardware limitations, other highly excited quartets and doublets were not considered. The state interaction step was performed by the RASSI-SO module<sup>21</sup> with the SOC integrals from the AMFI method.<sup>22</sup> The ANO-RCC basis sets,<sup>23–25</sup> including VTZP for Dy, VDZ for C and H as well as VDZP for other atoms, were used. All the calculations were carried out with the MOLCAS@UU, a version of MOLCAS 8.0 (ref. 26 and 27) which is freely distributed for academic users. The SINGLE\_ANISO module,<sup>28,29</sup> developed by Chibotaru *et al.*, was used to obtain the g-tensors, transition magnetic moments and other parameters characterizing the magnetic anisotropy.

### 3. Results and discussion

#### 3.1 Crystal structures

Compounds **Cl-1** and **CH<sub>3</sub>O-2** are crystallized in the triclinic space group *P*-1. **Cl-1** and **CH<sub>3</sub>O-2** have N<sub>2</sub>O<sub>6</sub> coordination environments. Each Dy(III) ion is surrounded by three negative-ion ligands and a neutral capping ligand (Phen), as shown in Fig. 1. The Dy–O distances are from 2.319 (7) to 2.369 (6) Å in **Cl-1** and from 2.305 (7) to 2.350 (5) Å in **CH<sub>3</sub>O-2**. Additionally, the Dy–N distances are 2.544 (8) Å and 2.586 (8) Å in **Cl-1** as well as 2.554 (6) Å and 2.571 (6) Å in **CH<sub>3</sub>O-2**. By using the SHAPE 2.1 software, the configurations of Dy(III) ions in **Cl-1** and **CH<sub>3</sub>O-2** were calculated (Table S2†), indicating that the compounds **Cl-1** and **CH<sub>3</sub>O-2** belong to an approximately square-antiprismatic (SAP, *D*<sub>4d</sub>) and trigonal dodecahedron (*D*<sub>2d</sub>) configuration, respectively.<sup>30</sup> The shortest interdinuclear Dy(III)···Dy(III) distances are 7.911 (6) Å in **Cl-1** and 10.742 (18) Å in **CH<sub>3</sub>O-2**, respectively.

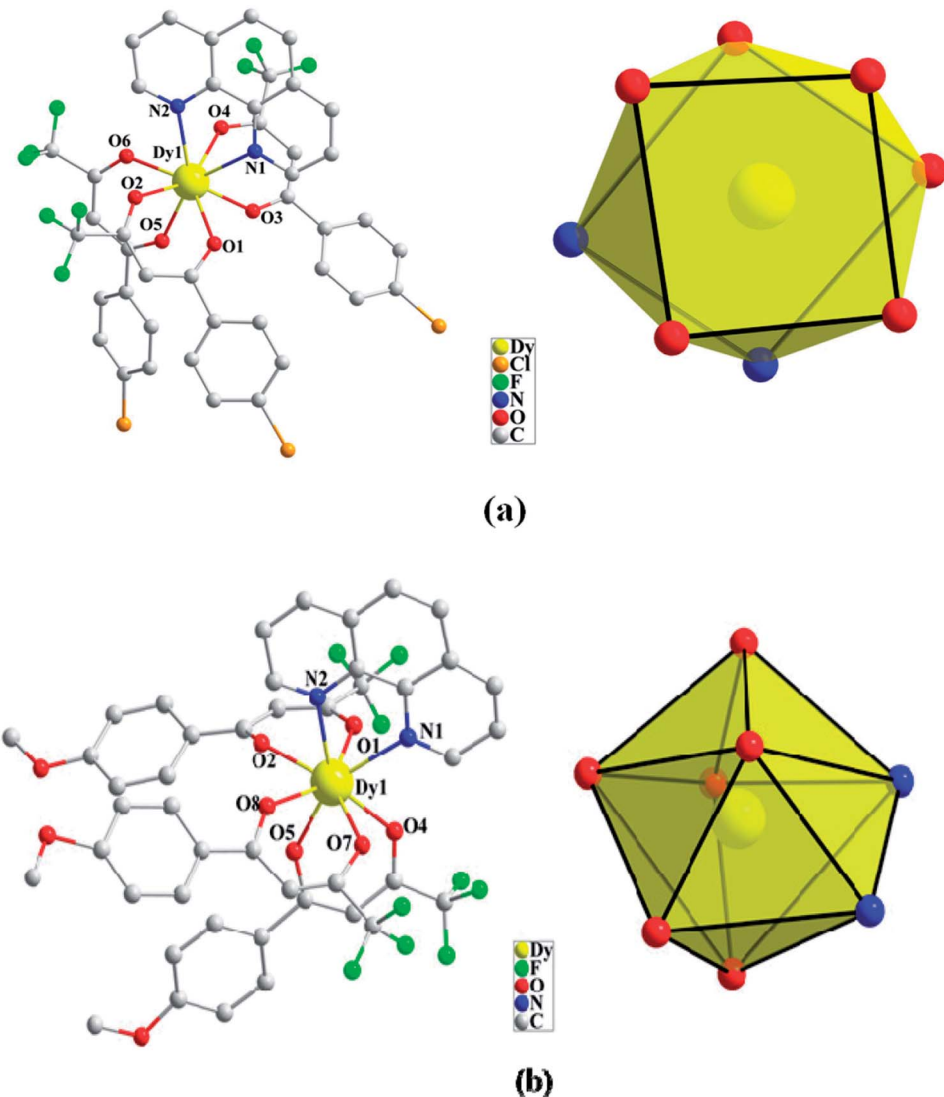
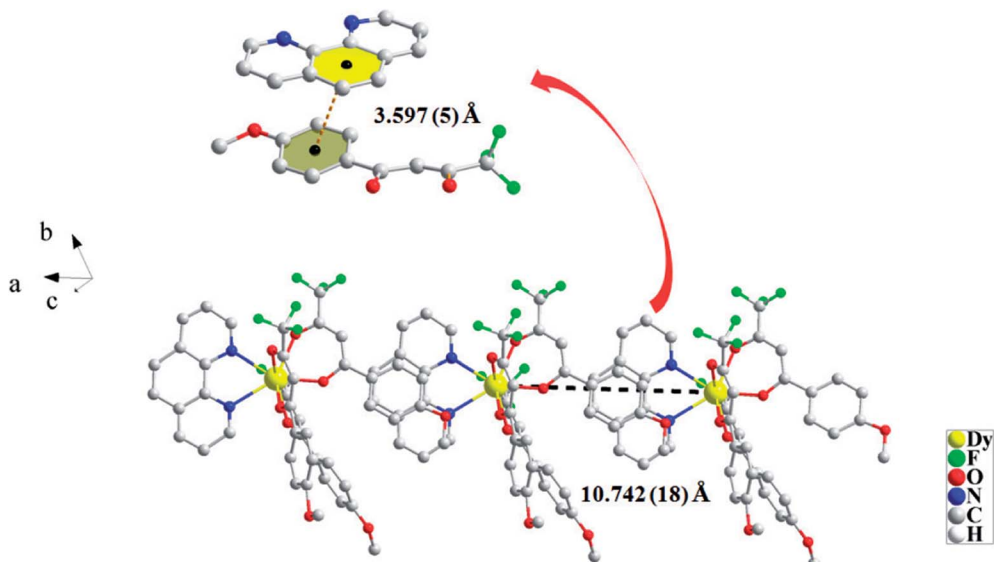
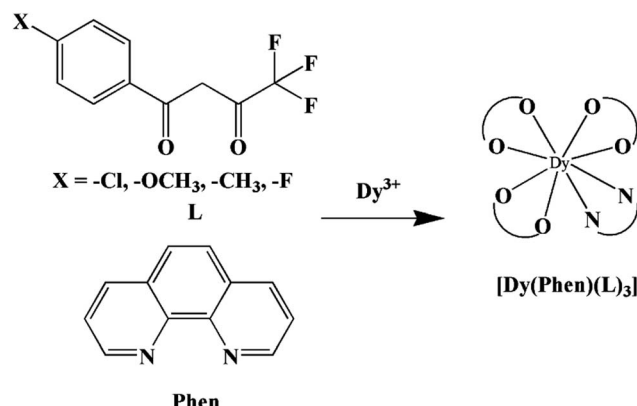


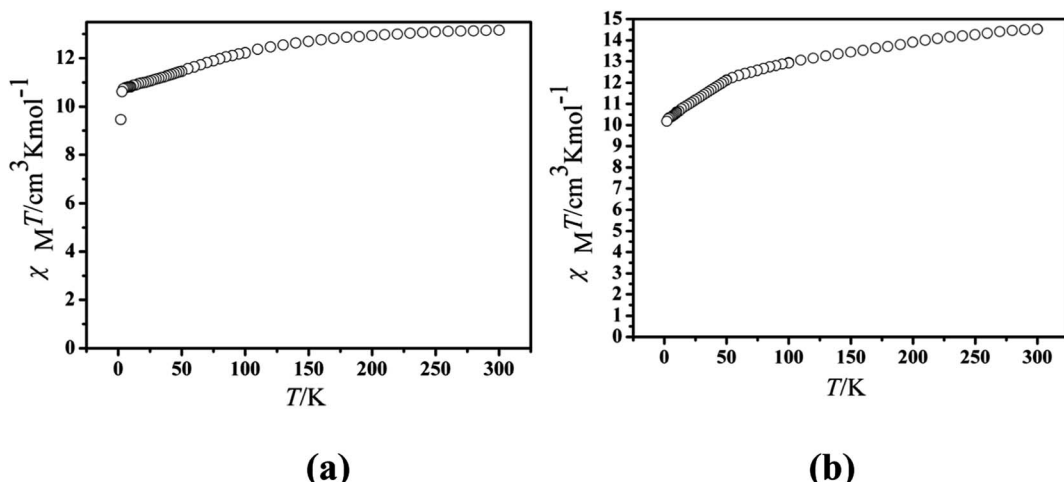
Fig. 1 Coordination environments of **Cl-1** (a) and **CH<sub>3</sub>O-2** (b) and the local coordination geometries of the Dy(III) ions of **Cl-1** (a) and **CH<sub>3</sub>O-2** (b); hydrogen atoms were omitted for clarity.



Fig. 2 Packing arrangement between two neutral molecules to form a 1D supramolecular chain in  $\text{CH}_3\text{O}-2$ .Scheme 1 The synthetic process for compounds with molecular formula  $\text{Dy}(\text{Phen})(\text{L})_3$ .

For  $\text{CH}_3\text{O}-2$ , the neutral molecules are assisted by weak  $\delta$ - $\delta$  stacking between the parallel interlayer (Fig. 2) to generate a 1D supramolecular chain, and the centroid distance is 3.597 (5) Å, from a slipped stacking and leading to the  $\text{Dy}(\text{III})\cdots\text{Dy}(\text{III})$  distance of 10.742 (18) Å. However, there is no obvious  $\delta$ - $\delta$  stacking or hydrogen bonding interaction in compound **Cl-1**.

In our previous works, the  $\beta$ -diketonate ligands with different substituent groups ( $-\text{F}/-\text{CH}_3$ ) were employed to obtain a series of mononuclear  $\text{Dy}(\text{III})$  compounds (Scheme 1). For  $\text{CH}_3\text{-}4$  (solvent) and  $\text{CH}_3\text{-}3$ , the latter has a trigonal dodecahedron ( $D_{2d}$ ) configuration of  $\text{Dy}(\text{III})$  ions, while  $\text{CH}_3\text{-}4$  (solvent) shows an approximately square antiprismatic (SAP,  $D_{4d}$ )  $\text{N}_2\text{O}_6$  coordination environment of  $\text{Dy}(\text{III})$  ions. The uncoordinated 1,4-dioxane molecules exist in  $\text{CH}_3\text{-}4$  (solvent). Interestingly, the compounds above have weak interactions between the neutral molecules. In  $\text{CH}_3\text{-}3$ , the neutral molecules are assisted by weak

Fig. 3 Temperature dependence of the  $\chi_M T$  product at 1000 Oe for compounds **Cl-1** (a) and  $\text{CH}_3\text{O}-2$  (b).

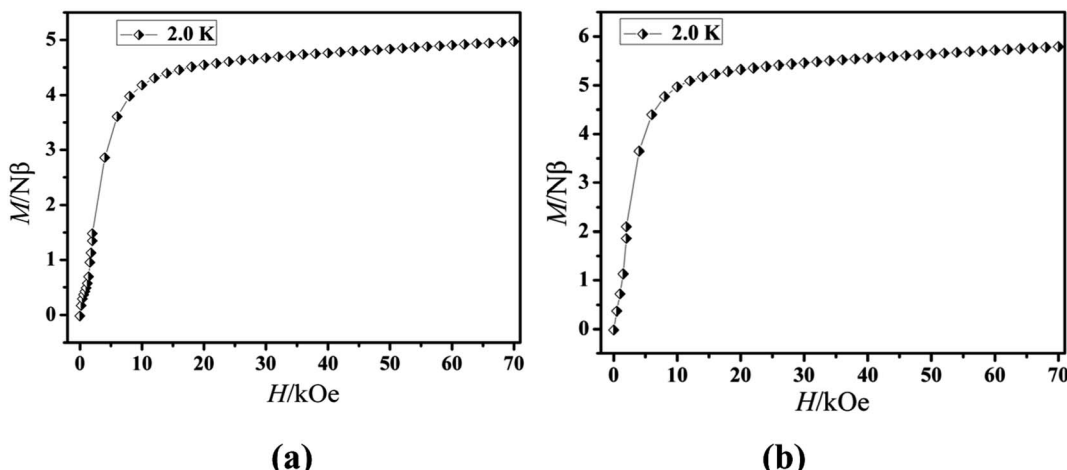


Fig. 4  $M$  vs.  $H$  plots at 2.0 K for compounds Cl-1 (a) and CH<sub>3</sub>O-2 (b).

$\pi \cdots \pi$  stacking between the parallel interlayer, and the centroid distance is 3.767 (6) Å, belonging to a slipped stacking and leading to the Dy(III)…Dy(III) distance of 9.193 (5) Å. In CH<sub>3</sub>O-2 (solvent), the neutral molecules are connected by weak C(171)–H(117)…O(7) interactions, leading to the Dy(III)…Dy(III) distance of 18.853 (2) Å. F-5 belongs to an approximately SAP configuration. For Cl-1, CH<sub>3</sub>-4 (solvent) and F-5, the CH<sub>3</sub>-4 (solvent) is more inclined toward the SAP configuration, calculated by utilizing the SHAPE 2.1 software. Cl-1 has the closest distance between the neutral molecules. In CH<sub>3</sub>O-2 and CH<sub>3</sub>-3, the former has the smaller deviation relative to a trigonal dodecahedron ( $D_{2d}$ ) configuration. The longer distance between the neutral molecules can be observed in CH<sub>3</sub>O-2. It is a remarkable fact that the maximum average Dy–N bond length is 2.563 Å (2) in CH<sub>3</sub>O-2. F-5 and CH<sub>3</sub>O-2 show similar average Dy–O bond lengths, which are smaller than Cl-1, CH<sub>3</sub>-3 and CH<sub>3</sub>-4 (solvent). The different types of weak interactions between the neutral molecules, configurations and bond lengths would result in different magnetic behaviors.

### 3.2 Magnetic properties

The magnetic experiments of Cl-1 and CH<sub>3</sub>O-2 were performed on polycrystalline samples. PXRD results of Cl-1 and CH<sub>3</sub>O-2 support the pure state of the bulk materials (Fig. S1†). The values of  $\chi_M T$  of Cl-1 and CH<sub>3</sub>O-2 are 13.16 cm<sup>3</sup> mol<sup>-1</sup> K and 14.51 cm<sup>3</sup> mol<sup>-1</sup> K at room temperature, respectively, which are close to the free-ion value of 14.17 cm<sup>3</sup> mol<sup>-1</sup> K for a single Dy(III) ion (<sup>6</sup>H<sub>15/2</sub>,  $S = 5/2$ ,  $L = 5$ ,  $J = 15/2$ ,  $g = 4/3$ ) (Fig. 3).<sup>13</sup> When cooled, the  $\chi_M T$  curves for compound Cl-1 decreased slowly in the range from 300 to 100 K. Subsequently, the  $\chi_M T$  products decreased sharply below 100 K to the minimum of 9.46 cm<sup>3</sup> mol<sup>-1</sup> K for Cl-1 and 11.75 cm<sup>3</sup> mol<sup>-1</sup> K for CH<sub>3</sub>O-2 at 1.8 K. In CH<sub>3</sub>O-2, on lowering the temperature, the  $\chi_M T$  product decreased gradually and more rapidly below 50 K. These behaviors could be ascribed to crystal field splitting, particularly the progressive quenching of excited Dy(III) Stark sublevels and/or weak intermolecular dipole–dipole effects.<sup>32</sup>

The magnetization of the two compounds from zero dc field to 70 kOe at different temperatures is shown in Fig. 4. The

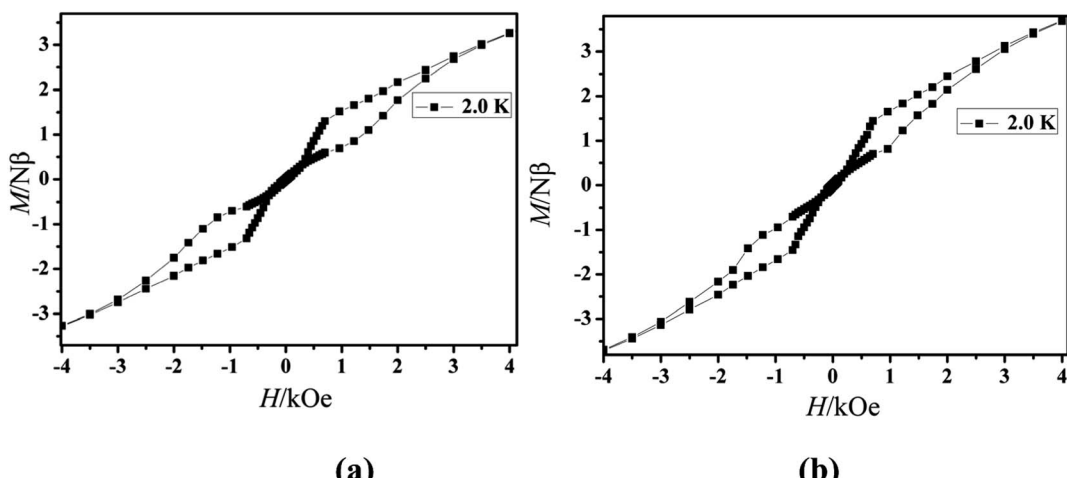


Fig. 5  $M$  versus  $H$  data of Cl-1 (a) and CH<sub>3</sub>O-2 (b) at 2.0 K.



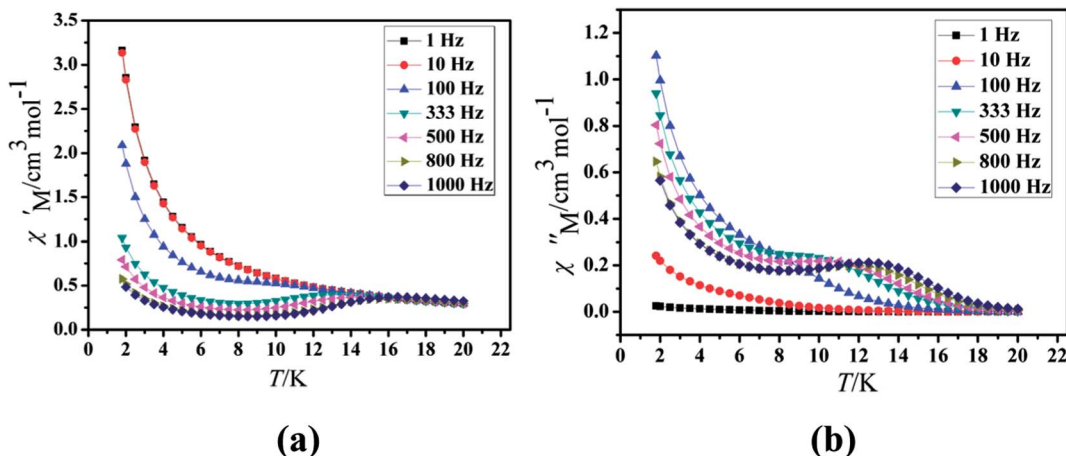


Fig. 6 Temperature dependence of the in-phase ( $\chi'$ , a) and out-of-phase ( $\chi''$ , b), respectively, of the ac susceptibility for Cl-1 under the zero-dc field.

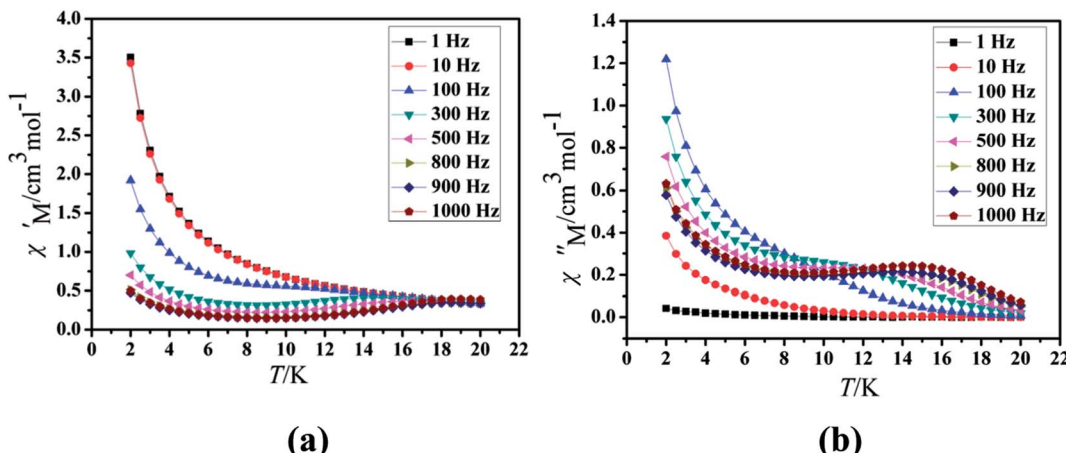


Fig. 7 Temperature dependence of the in-phase ( $\chi'$ , a) and out-of-phase ( $\chi''$ , b), respectively, of the ac susceptibility for  $\text{CH}_3\text{O}$ -2 under the zero-dc field.

magnetization of **Cl-1** and **CH<sub>3</sub>O-2** at 2 K increased upon application of an external field to a maximum of 4.97 N $\beta$  and 5.79 N $\beta$ . The maximum values in **Cl-1** and **CH<sub>3</sub>O-2** at 7 T largely deviate from the expected saturation point of 10 N $\beta$ , consisting of the magnetic anisotropy and crystal field effects at the dysprosium center, which dispel the 16-fold degeneration of the <sup>6</sup>H<sub>15/2</sub> ground state.<sup>33</sup> The  $M$  versus  $H$  data exhibit obvious butterfly-shaped hysteresis loops at 2 K for **Cl-1** and **CH<sub>3</sub>O-2** (Fig. 5), indicating the fast zero-field relaxation between the two ground states.

Under the oscillating field of 3.5 Oe, the zero-field AC susceptibility experiments were determined in the range of 1.8–20 K and at frequencies of 1, 10, 100, 333, 500, 800 and 1000 Hz in **Cl-1**. However, for **CH<sub>3</sub>O-2**, zero-field AC susceptibilities were measured in the range of 2–18 K and at frequencies of 1, 10, 100, 300, 500, 800, 900 and 1000 Hz. Both in-phase ( $\chi'$ ) and out-of-phase ( $\chi''$ ) susceptibilities in compound **Cl-1** and **CH<sub>3</sub>O-2** showed significant temperature dependence peaks at a relatively high-temperature range (Fig. 6 and 7), which clearly

indicates the slow relaxation of magnetization. When cooled,  $\chi'$  and  $\chi''$  increased again at lower temperatures; such a situation could be due to the emergence of quantum tunneling of magnetization (QTM) without an extra dc field, which often occurs in Ln(III)-based SMMs or SIMs (Table 1).<sup>34</sup>

Furthermore, the frequency-dependent ac data for compounds **Cl-1** and **CH<sub>3</sub>O-2** were characterized in the absence of a dc field at various temperatures; the peaks of the  $\chi''$  plots gradually shifted with the frequency sequence from middle to high, indicating that the  $\chi''$  of compounds **Cl-1** and **CH<sub>3</sub>O-2** manifested frequency dependence in the selected temperature range (Fig. 8 and 9). The fitting of the Cole–Cole plots ( $\chi'$  M vs.  $\chi''$ ) for **Cl-1** and **CH<sub>3</sub>O-2** (Fig. 10 and 11) with the Debye model<sup>13</sup> presented a non-symmetric semicircle, which indicates the presence of a relatively moderate distribution of relaxation time ( $0.011 < \alpha < 0.181$  for **Cl-1** and  $0.007 < \alpha < 0.161$  for **CH<sub>3</sub>O-2**) (Table 3 and 4). For the relaxation time products under 0 Oe, the direct process can be neglected. The  $\ln(\tau)$  versus  $1/T$  plots for compound **Cl-1** and **CH<sub>3</sub>O-2** presented some curvature (Fig. 12),

**Table 1** The notable examples of  $\text{DyN}_2\text{O}_6$  mononuclear dysprosium compounds, namely  $[\text{Dy}(\text{Phen})(\text{L})_3]$ , based on the  $\beta$ -diketonate ligands with different substituent groups ( $-\text{Cl}$ ,  $-\text{CH}_3$ ,  $-\text{CH}_3\text{O}$ ,  $-\text{F}$ ) at the 4-position

L	$d_{\text{Dy}-\text{O}}$	$d_{\text{Dy}-\text{N}}$	$d_{\text{Dy}\cdots\text{Dy}}$	Symmetry	$U_{\text{eff}}$ (K)	Ref.	Name
	2.337 (2)	2.538 (3)	9.355 (11)	$D_{2\text{d}}$	63.56 K/67.05 K (0 Oe) 118.50 K (1200 Oe)	13b	<b>CH<sub>3</sub>-3</b>
	2.329 (4)	2.553 (5)	9.193 (10)	$D_{4\text{d}}$	102.82 K/95.88 K (0 Oe) 164.55 (1200 Oe)	13b	<b>CH<sub>3</sub>-4 (solvent)</b>
solvent							
	2.311 (3)	2.579 (3)	9.679 (8)	$D_{4\text{d}}$	91.70 K (1200 Oe)	31	<b>F-5</b>
	2.339 (6)	2.562 (8)	7.911 (6)	$D_{4\text{d}}$	151 (0 Oe)	Here	<b>Cl-1</b>
	2.322 (5)	2.563 (6)	10.742 (13)	$D_{2\text{d}}$	190.7 (0 Oe)	Here	<b>CH<sub>3</sub>O-2</b>

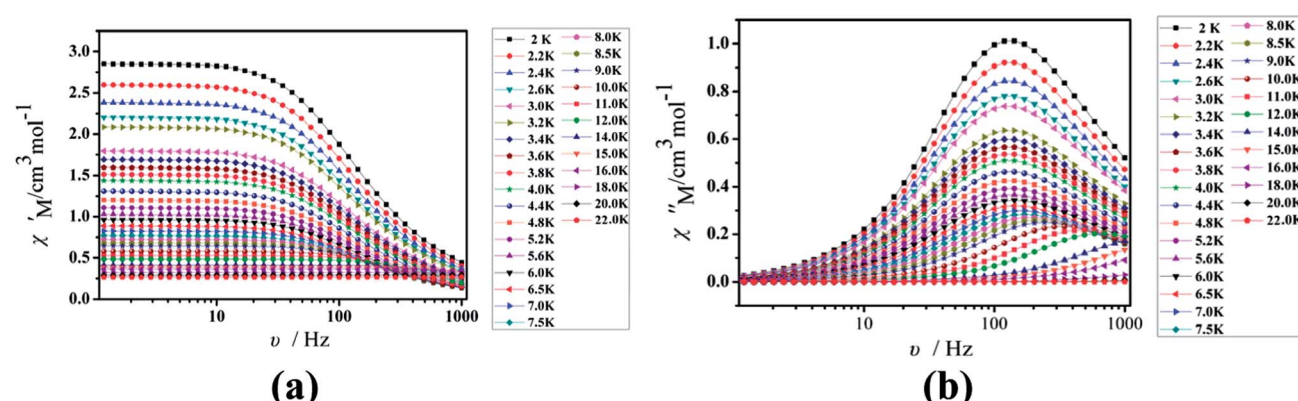


Fig. 8 Frequency dependence of the in-phase ( $\chi'$ , a) and out-of-phase ( $\chi''$ , b) of the ac susceptibility for **Cl-1** under the zero-dc field.

indicating that the dynamics cannot be properly modelled by assuming a simple Orbach mechanism. Therefore, the total relaxation rates mainly reflect the Orbach process, Raman process and QTM process, using the following equation (eqn (1)):

$$\tau^{-1} = \tau_{\text{QTM}}^{-1} + CT^n + \tau_0^{-1} \exp(-U_{\text{eff}}/kT) \quad (1)$$

where  $\tau$  is the inverse of the ac frequency,  $T$  is the temperature of the maximum in the ac signal,  $U_{\text{eff}}$  is the effective energy barrier,  $k$  is Boltzmann's constant.  $\tau_{\text{QTM}}$ ,  $C$ , and  $\tau_0$  are the fitting parameters of the different relaxation mechanisms. In the absence of a static field, the independence of the relaxation

time at low temperatures for compounds **Cl-1** and **CH<sub>3</sub>O-2** are indicative of QTM relaxation processes. The fit in the temperature range  $T = 2.0\text{--}22.0$  K for compound **Cl-1** by eqn (1) resulted in  $\tau_{\text{QTM}} = 0.001$  s,  $n = 4.97$ ,  $C = 1.33 \times 10^{-3} \text{ s}^{-1} \text{ K}^{-4.97}$ ,  $\tau_0 = 1.44 \times 10^{-8}$  s, and an effective energy barrier of  $U_{\text{eff}} = 105.431 \text{ cm}^{-1}$  (151.1 K). The fit in the temperature range  $T = 2.0\text{--}20.0$  K for compound **CH<sub>3</sub>O-2** by eqn (1) resulted in  $\tau_{\text{QTM}} = 0.001$  s,  $n = 4.06$ ,  $C = 8.58 \times 10^{-2} \text{ s}^{-1} \text{ K}^{-4.06}$ ,  $\tau_0 = 5.08 \times 10^{-9}$  s, and an effective energy barrier of  $U_{\text{eff}} = 132.5 \text{ cm}^{-1}$  (190.7 K).

The different local symmetries and the bond distances contribute to differing ligand fields, further resulting in diverse dynamic magnetic behaviors.<sup>13b,35</sup> The **CH<sub>3</sub>-4** (solvent) with an approximately square antiprismatic (SAP,  $D_{4\text{d}}$ )  $\text{N}_2\text{O}_6$



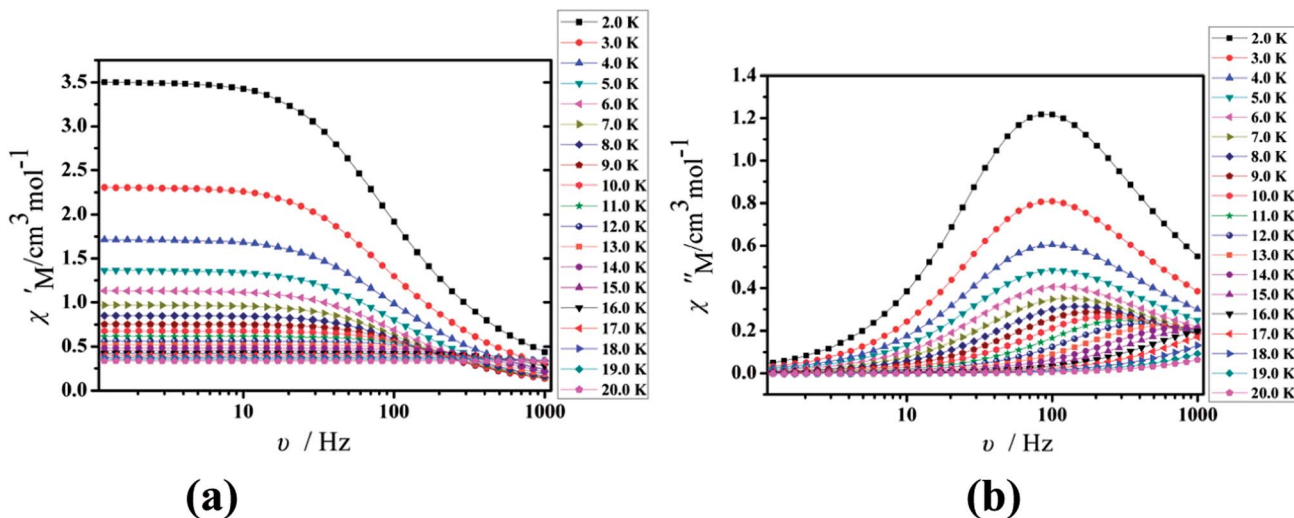


Fig. 9 Frequency dependence of the in-phase ( $\chi'$ , a) and out-of-phase ( $\chi''$ , b) of the ac susceptibility for  $\text{CH}_3\text{O-2}$  under the zero-dc field.

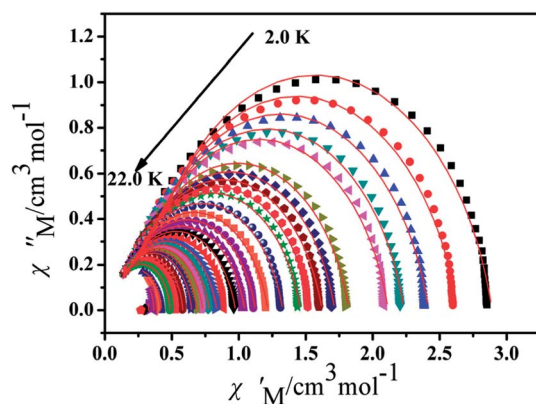


Fig. 10 Cole–Cole plots for Cl-1 from 2.0 K to 22.0 K using the ac susceptibility data. The solid lines are the best fits for the generalized Debye model between 2.0 K and 22.0 K.

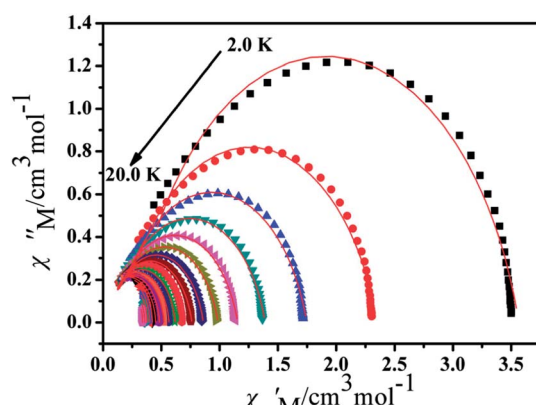


Fig. 11 Cole–Cole plots for  $\text{CH}_3\text{O-2}$  from 2.0 K to 20.0 K using the ac susceptibility data. The solid lines are the best fits for the generalized Debye model between 2.0 K and 20.0 K.

coordination environment exhibited more excellent properties than  $\text{CH}_3\text{-3}$  with a trigonal dodecahedron ( $D_{2d}$ ) configuration.<sup>35</sup> However, the results in the present cases are in contrast to the explanation above, which verifies that the relaxation magnetism

Table 2 *Ab initio* computed relative energies (in  $\text{cm}^{-1}$ ), principal values of the g-tensors and averaged transition magnetic moments  $\mu_{\text{QTM}}$  (in  $\beta$ ) of the four lowest  $\text{KD}_s$  of the compounds studied in this work

	Cl-1	$\text{CH}_3\text{O-2}$
$\text{KD}_0$	$E$	0.000
	$g_z$	19.5623
	$g_x$	$0.8671 \times 10^{-2}$
	$g_y$	$0.1788 \times 10^{-1}$
	$g_{xy}$	$0.1987 \times 10^{-1}$
	$g_{xy}/g_z$	$0.1016 \times 10^{-2}$
	$\mu_{\text{QTM}}$	$0.4425 \times 10^{-2}$
$\text{KD}_1$	$E$	126.712 (105.431) <sup>a</sup>
	$g_z$	15.4850
	$g_x$	$0.5304 \times 10^{+00}$
	$g_y$	$0.1117 \times 10^{+01}$
	$g_{xy}$	$0.1237 \times 10^{+01}$
	$g_{xy}/g_z$	$0.7988 \times 10^{-1}$
	$\mu_{\text{QTM}}$	$0.2746 \times 10^{+00}$
$\text{KD}_2$	$E$	151.045
	$g_z$	17.6519
	$g_x$	$0.4178 \times 10^{+00}$
	$g_y$	$0.1481 \times 10^{+01}$
	$g_{xy}$	$0.1538 \times 10^{+01}$
	$g_{xy}/g_z$	$0.8716 \times 10^{-1}$
	$\mu_{\text{QTM}}$	$0.3164 \times 10^{+00}$
$\text{KD}_3$	$E$	177.793
	$g_z$	13.8539
	$g_x$	$0.3264 \times 10^{+01}$
	$g_y$	$0.3822 \times 10^{+01}$
	$g_{xy}$	$0.5026 \times 10^{+01}$
	$g_{xy}/g_z$	$0.3628 \times 10^{+00}$
	$\mu_{\text{QTM}}$	$0.1181 \times 10^{+01}$

<sup>a</sup> Experimental  $U_{\text{eff}}$  is shown in parentheses.

Table 3 The results of preliminary ESP (in a.u.) analysis

	Cl-1	CH <sub>3</sub> O-2
ESP <sub>(equ)</sub> /ESP <sub>(ax)</sub>	0.723	0.701
ESP <sub>(ax)</sub>	1.082	1.162
ESP <sub>(equ)</sub>	0.783	0.814
ESP <sub>(equ_N)</sub> <sup>a</sup>	0.225	0.220
ESP <sub>(equ_O)</sub> <sup>b</sup>	0.557	0.594

<sup>a</sup> Contributions from the equatorial N atoms. <sup>b</sup> Contributions from the equatorial O atoms.

incompletely depends on the coordination symmetry of the Dy<sup>III</sup> centers. Accordingly, the magnetism of dysprosium-based SMMs might be simultaneously dominated by complicated factors including local symmetry, electrostatics, *etc.*<sup>10b,36</sup>

In our recent work, a similar phenomenon was observed in the two  $\beta$ -diketone mononuclear Dy<sup>III</sup> compounds, formulated as Dy(BTFA)<sub>3</sub>(H<sub>2</sub>O)<sub>2</sub> ( $D_{2d}$ ) and Dy(BTFA)<sub>3</sub>(bpy) ( $D_{4d}$ ) (BTFA = 3-benzoyl-1,1,1-trifluoroacetone, bpy = 2,2'-bipyridine).<sup>10b</sup> As noticed, compound Dy(BTFA)<sub>3</sub>(H<sub>2</sub>O)<sub>2</sub> possesses a higher effective barrier than Dy(BTFA)<sub>3</sub>(bpy), despite Dy(BTFA)<sub>3</sub>(H<sub>2</sub>O)<sub>2</sub> exhibiting a lower geometrical symmetry of the Dy<sup>III</sup> ion. This is likely attributable to different charge distributions around the Dy<sup>III</sup> ions in both compounds, which compensate for the discrepancy of the geometrical symmetries and is responsible for the disparities in magnetic anisotropy, as well as energy barrier and slow relaxation behavior between the two compounds. However, the conjecture above urgently needs studies for an in-depth understanding of the significative magneto-structural correlation.

According to the Dy<sup>III</sup> coordination spheres, the compounds are slightly distorted, with the following order: F-5 > Cl-1 > CH<sub>3</sub>-4 (solvent); CH<sub>3</sub>-3 > CH<sub>3</sub>O-2. The shortest intermolecular distance between Dy<sup>III</sup> ions is 7.911 (6) Å in Cl-1. However, there are no obvious  $\delta$ - $\delta$  stacking or hydrogen bonding interactions in Cl-1, probably resulting in the weakening of the QTM relaxation process from the intermolecular interactions. CH<sub>3</sub>O-2 shows shorter bond lengths for Dy-N and Dy-O than CH<sub>3</sub>-3 and a smaller degree of distortion, indicating the strong charge density around the metal ions and further generating enhanced uniaxial magnetic anisotropy. Finally, these different effective energy barriers ( $\Delta E/k_B$ ) have the following order: CH<sub>3</sub>O-2 > Cl-1 > CH<sub>3</sub>-4 (solvent) > CH<sub>3</sub>-3 > F-5.

### 3.3 Theoretical analysis

The effective energy barrier for the reversal of magnetization,  $U_{\text{eff}}$ , is a popular parameter that is used to characterize the SMM properties of the compounds. However, only within the Orbach process is  $U_{\text{eff}}$  clearly defined in principle. In the early stages of the SMM, the compounds were usually polynuclear transition metal structures where the Orbach process dominated the magnetic relaxation; since then,  $U_{\text{eff}}$  has become popular in the field of SMM. However, in the case of mononuclear SIMs, several relaxation processes, including both Orbach and others of QTM, direct as well as Raman, exist simultaneously.<sup>37-39</sup> Thus, the magnetic relaxation in Ln-based SIMs is not naturally dominated by the Orbach process and the necessary condition for the observation of SMM behavior is the effective suppression of all the fast relaxation process.<sup>38,39</sup> Among all the fast relaxation processes, the quantum tunnelling of magnetization (QTM) within the ground state is the most effective and thus its suppression is the first target. Irrespective of various sources, the rate of QTM scales as the square of the so-called tunnel splitting  $\Delta_{\text{tun}}$ .<sup>37-40</sup> For Kramers ions, *e.g.*, Dy<sup>III</sup>,  $D_{\text{tun}}$  is forced to be zero under the strict absence of a magnetic field due to time-reversal symmetry; however, small internal magnetic fields actually exist with different sources.<sup>38</sup> Therefore  $\Delta_{\text{tun}}$  in Kramers systems is induced *via* the Zeeman interaction (eqn (1a)) between the transversal fields ( $H_X$  and  $H_Y$ ) and the corresponding components of the magnetic moments  $\vec{\mu}$  of the same directions ( $\mu_X$  and  $\mu_Y$ ).<sup>37-41</sup>

$$\Delta_{\text{tun}} = \left[ (\mu_X H_X)^2 + (\mu_Y H_Y)^2 \right]^{1/2} = \frac{1}{2} \left[ \beta (g_X^2 H_X^2 + g_Y^2 H_Y^2) \right]^{1/2} \quad (1a)$$

$$\mu_{\alpha} = -\left\langle -n \left| \beta g_{\alpha} \hat{S}_{\alpha} \right| n \right\rangle = -\frac{1}{2} g_{\alpha} \beta \quad \alpha = X, Y, Z \quad (1b)$$

$$g_{\alpha} = 2 \langle -n | \hat{\mu}_{\alpha} | n \rangle / \beta \quad \alpha = X, Y, Z \quad (1c)$$

Theoretically, each Kramers doublet (KD) could be associated with an effective spin (pseudospin)  $S = 1/2$ .<sup>28,37,38</sup> The magnetic moment of such pseudospin is determined by its principal values of the g-tensors as shown in eqn (1b).<sup>37,38</sup> Clearly, small values of the transversal  $g_X$  and  $g_Y$  (eqn (1c)) of the ground KD, *i.e.*, KD<sub>0</sub>, will lead to a low magnitude of  $\Delta_{\text{tun}}$  and

Table 4 The negative charges (in |e|) from *ab initio* calculations and the related Dy–O/N bond lengths (in Å) of the atoms in the first sphere<sup>a</sup>

Cl-1	O <sub>3</sub> -ax	O <sub>5</sub> -ax	O <sub>2</sub> -ax	O <sub>4</sub> -ax	O <sub>6</sub> -equ	O <sub>7</sub> -equ	N <sub>8</sub> -equ	N <sub>9</sub> -equ
Charge	0.696	0.679	0.690	0.687	0.698	0.699	0.339	0.326
Dy–O/N	2.319 (7)	2.352 (6)	2.369 (6)	2.339 (6)	2.330 (6)	2.321 (6)	2.544 (8)	2.586 (8)
CH <sub>3</sub> O-2	O <sub>2</sub> -ax	O <sub>7</sub> -ax	O <sub>3</sub> -ax	O <sub>5</sub> -ax	O <sub>4</sub> -equ	O <sub>6</sub> -equ	N <sub>8</sub> -equ	N <sub>9</sub> -equ
Charge	0.722	0.764	0.704	0.710	0.764	0.697	0.332	0.304
Dy–O/N	2.350 (5)	2.307 (5)	2.318 (5)	2.305 (7)	2.337 (6)	2.312 (6)	2.554 (6)	2.571 (6)

<sup>a</sup> “-ax” indicates the atoms at the axial positions and “-equ” means the atoms at equatorial positions.



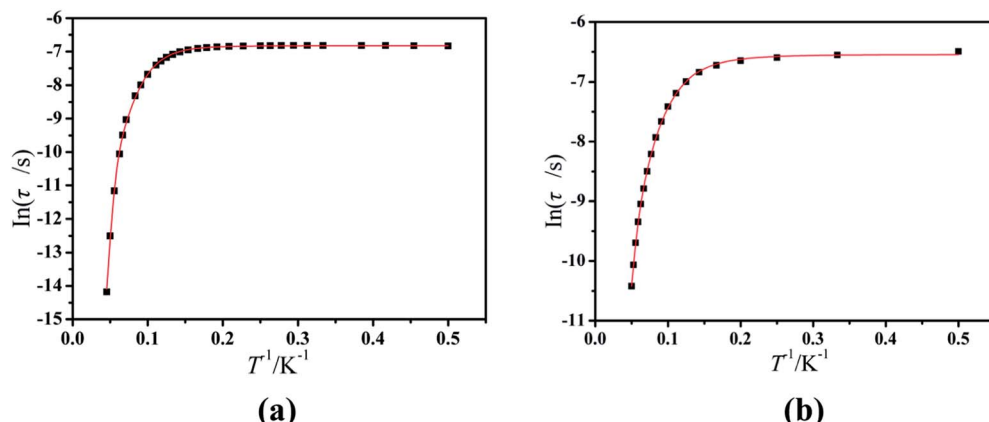


Fig. 12 Magnetization relaxation time ( $\ln(\tau)$ ) versus  $T^{-1}$  plots under a zero dc field for Cl-1 (a) and CH<sub>3</sub>O-2 (b). The solid red line represents the best fitting to the multiple relaxation processes (eqn (1), see text for parameters).

thus zero-field SIM behavior could exist if the value of  $g_{XY}$  for KD<sub>0</sub> is small enough.<sup>42</sup> Besides the principal  $g$  values of each KD, *ab initio* calculations also provide the averaged absolute value of the transversal magnetic moments,  $\mu_{\text{QTM}}$ , which could also be used to measure the strength of QTM. As shown in Table 2, the  $g_{XY}$  values of KD<sub>0</sub> are  $0.1987 \times 10^{-1}$  and  $0.5421 \times 10^{-2}$  for Cl-1 and CH<sub>3</sub>O-2, respectively. According to previous results from Ruiz *et al.*,<sup>17</sup> zero-field SIM behavior could occur if the  $g_{XY}$  of KD<sub>0</sub> is smaller than  $0.15 \times 10^{-1}$  for mononuclear Dy(III) compounds. Clearly, this criterion is fulfilled in the case of CH<sub>3</sub>O-2 and, although a little bit larger, the  $g_{XY}$  of KD<sub>0</sub> of Cl-1 is also quite close to this value. Therefore our *ab initio* results do suggest the existence of zero-field SIM properties in these two compounds, which is consistent with the experimental observation based on ac susceptibility measurements.

Due to the smaller value of  $g_{XY}$  of KD<sub>0</sub>, the SIM property of CH<sub>3</sub>O-2 is theoretically predicted to be superior to that of Cl-1. This theoretical prediction is also in line with the higher  $U_{\text{eff}}$  of CH<sub>3</sub>O-2 obtained from the fitting of the experimental data. In many cases of Ln-SIMs, the energy of the first excited KD, *i.e.*, KD<sub>1</sub>, is closely related to the  $U_{\text{eff}}$ . In the two compounds here, the energies of KD<sub>1</sub> are indeed close to the experimental  $U_{\text{eff}}$ :  $126.7 \text{ cm}^{-1}$  vs.  $105.4 \text{ cm}^{-1}$  for Cl-1 and  $152.8 \text{ cm}^{-1}$  vs.  $132.5 \text{ cm}^{-1}$  for CH<sub>3</sub>O-2. Moreover, the energy of KD<sub>1</sub> for CH<sub>3</sub>O-2

is also higher than that of Cl-1. Thus, the reliability of our *ab initio* results is verified again in terms of energies of KD<sub>1</sub>.

As shown in our previous results,<sup>14,18,19</sup> the desired electronic structure, which is suitable for the ideal SIM properties of Dy(III) systems, could be approached *via* an electrostatic route due to the oblate electron density of the Dy(III) ion; *i.e.*, the axial electrostatic potential (ESP) should exceed the equatorial one as much as possible.<sup>6,31,40,43</sup> According to the orientation of the magnetic easy axis (Fig. 13), the eight atoms of the first sphere could be collected into two groups: (1) axial atoms consisting of the four oxygen atoms (O2, O3, O4 and O5 for Cl-1) that lie along the axial direction; (2) equatorial atoms consisting of the two nitrogen atoms and the residual two oxygen atoms (N8, N9, O6 and O7 for Cl-1). With *ab initio* atomic charge, we could approximate the axial ESP felt by the Dy(III) ion, *i.e.*, ESP<sub>(ax)</sub>, with the sum of the contribution from the four axial atoms. Similarly, the equatorial ESP, *i.e.*, ESP<sub>(equ)</sub>, could be approximated as the collection of the contribution from the four equatorial atoms. As shown before,<sup>31,40,43</sup> the lower value of the ratio ESP<sub>(equ)</sub>/ESP<sub>(ax)</sub> indicates the higher degree of the excess of the axial ESP over the equatorial, and thus it should lead to the electronic structure, which is more suitable for the ideal SIM properties.

As shown in Table 3, the ESP<sub>(equ)</sub>/ESP<sub>(ax)</sub> ratio of CH<sub>3</sub>O-2 is 0.701, clearly lower than that of Cl-1 (0.723). Thus, the superior

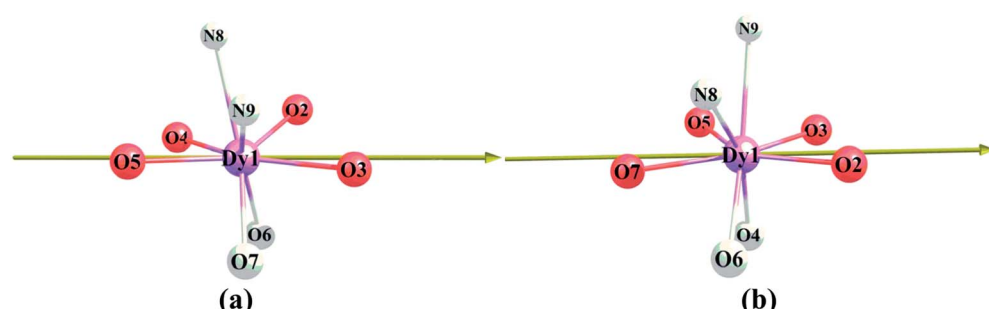


Fig. 13 Direction of the *ab initio* magnetic easy axis of the ground KDs of the compounds (only the central Dy(III) and first sphere are shown for the sake of clarity, the equatorial atoms are shaded).

SIM property of **CH<sub>3</sub>O-2** should originate from the more suitable ESP felt by the central Dy(III) ion when compared with **1**. In detail, the difference in ESP<sub>(equ)</sub> of these two compounds is 0.03 a.u., which is clearly smaller than the corresponding difference in ESP<sub>(ax)</sub> (0.08 a.u.). In other words, the different amounts of ESP<sub>(ax)</sub> of these two compounds should play the central role in their differences in terms of SIM properties. When making a further analysis of the charges and distances to the central ion (Table 4), the averaged charges and distances to the central Dy(III) ion are 0.725 |e| and 2.320 Å, respectively, for **CH<sub>3</sub>O-2**. In the case of **Cl-1**, the averaged charges and distances are 0.688 |e| and 2.345 Å, respectively. Therefore the larger amount of ESP<sub>(ax)</sub> for **CH<sub>3</sub>O-2** arises from the synergic effect of the more negative charge and shorter Dy–O distances of the axial O atoms of the first sphere. Of course, these charges and distances could be influenced by functional groups outside the first sphere, *e.g.*, –Cl and –OCH<sub>3</sub>.

## 4. Conclusion

Two mononuclear compounds, [Dy(Phen)(Cl-tcpb)<sub>3</sub>] (**Cl-1**) and [Dy(Phen)(CH<sub>3</sub>O-tmpd)<sub>3</sub>] (**CH<sub>3</sub>O-2**), were synthesized based on  $\beta$ -diketonate ligands (Cl-tcpb = 1-(4-chlorophenyl)-4,4,4-trifluoro-1,3-butanedione and CH<sub>3</sub>O-tmpd = 4,4,4-trifluoro-1-(4-methoxyphenyl)-1,3-butanedione) with different substituent groups (–Cl/–OCH<sub>3</sub>) and auxiliary ligand 1,10-phenanthroline (Phen). The Dy(III) ions in **Cl-1** have approximately square-antiprismatic (SAP,  $D_{4d}$ ) N<sub>2</sub>O<sub>6</sub> coordination environments. The coordination geometry of Dy(III) ions in **CH<sub>3</sub>O-2** can be best described as a trigonal dodecahedron ( $D_{2d}$ ). The dynamic magnetic investigations showed that both compounds exhibited SMM behavior in zero dc field, while the effective magnetization relaxation barriers increased progressively from 105.4 cm<sup>–1</sup> (151.1 K) for **Cl-1** to 132.5 cm<sup>–1</sup> (190.7 K) for **CH<sub>3</sub>O-2**. **CH<sub>3</sub>O-2** possessed a higher effective barrier than **Cl-1**, despite **Cl-1** exhibiting a higher geometrical symmetry of the Dy(III) ion. Moreover, the energy of KD<sub>1</sub> of **CH<sub>3</sub>O-2** was also higher than that of **Cl-1**. The zero-field SIM behaviors, as well as the difference in  $U_{eff}$ , of these two compounds were reproduced by *ab initio* calculations. Further studies from the viewpoint of electrostatic potential demonstrated that the larger axial electrostatic potential (ESP) felt by the central Dy(III) ion of **CH<sub>3</sub>O-2** is responsible for its better SIM properties when compared with **Cl-1**. The larger amount of ESP<sub>(ax)</sub> of **CH<sub>3</sub>O-2** arises from the synergic effect of the more negative charge and shorter Dy–O distances of the axial O atoms of the first sphere. Beyond all doubt, these charges and distances could be affected by functional groups outside the first sphere, *e.g.*, –Cl and –OCH<sub>3</sub>.

## Conflicts of interest

There are no conflicts to declare.

## Acknowledgements

We gratefully acknowledge financial support from the National Natural Science Foundation of China (Nos. 21703002,

21103137), the 61th China Postdoctoral Science Foundation funded project (2017M610646), the Doctoral Scientific Research Starting Foundation of Baoji University of Arts and Science (No. ZK2017024) and the Fund of Northwest University (334100048).

## Notes and references

- 1 R. Sessoli, D. Gatteschi, A. Caneschi and M. A. Novak, *Nature*, 1993, **365**, 141–143.
- 2 (a) D. Gatteschi, R. Sessoli, J. Villain, *Molecular Nanomagnets*, Oxford University Press, Oxford, 2006; (b) D. G. C. Benelli, *Introduction to Molecular Magnetism. From Transition Metals to Lanthanide*, Wiley-VCH, Weinheim, 2015; (c) G. A. Timco, S. Carretta, F. Troiani, F. Tuna, R. J. Pritchard, C. A. Muryn, E. J. L. McInnes, A. Ghirri, A. Candini, P. Santini, G. Amoretti, M. Affronte and R. E. P. Winpenny, *Nat. Nanotechnol.*, 2009, **4**, 173–178; (d) S. G. McAdams, A. M. Ariciu, A. K. Kostopoulos, J. P. S. Walsh and F. Tuna, *Coord. Chem. Rev.*, 2017, **346**, 216–239; (e) S. T. Liddle and J. van Slageren, *Chem. Soc. Rev.*, 2015, **44**, 6655–6669; (f) F. Pointillart, O. Cador, B. Le Guennic and L. Ouahab, *Coord. Chem. Rev.*, 2017, **346**, 150–175; (g) S. Demir, I. R. Jeon, J. R. Long and T. D. Harris, *Coord. Chem. Rev.*, 2015, **289**, 149–176; (h) Y.-S. Meng, S.-D. Jiang, B.-W. Wang and S. Gao, *Acc. Chem. Res.*, 2016, **49**, 2381–2389.
- 3 (a) C. Benelli and D. Gatteschi, *Chem. Rev.*, 2002, **102**, 2369–2388; (b) R. Skomski, *Simple models of magnetism*, Oxford University Press, New York 2008; (c) D. N. Woodruff, R. E. Winpenny and R. A. Layfield, *Chem. Rev.*, 2013, **113**, 5110–5148; (d) J. D. Rinehart and J. R. Long, *Chem. Sci.*, 2011, **2**, 2078–2085; (e) P. Zhang, Y.-N. Guo and J.-K. Tang, *Coord. Chem. Rev.*, 2013, **257**, 1728–1763.
- 4 (a) J. Liu, Y.-C. Chen, J.-L. Liu, V. Vieru, L. Ungur, J.-H. Jia, L. F. Chibotaru, Y. Lan, W. Wernsdorfer, S. Gao, X.-M. Chen and M.-L. Tong, *J. Am. Chem. Soc.*, 2016, **138**, 5441–5450; (b) Y.-C. Chen, J.-L. Liu, L. Ungur, J. Liu, Q.-W. Li, L.-F. Wang, Z.-P. Ni, L. F. Chibotaru, X.-M. Chen and M.-L. Tong, *J. Am. Chem. Soc.*, 2016, **138**, 2829–2837; (c) J. J. Le Roy, L. Ungur, I. Korobkov, L. F. Chibotaru and M. Murugesu, *J. Am. Chem. Soc.*, 2014, **136**, 8003–8010; (d) M. Li, H.-P. Wu, Y. Qi, H.-S. Ke, B. Yin, Q. Shi, W.-Y. Wang, Q. Wei, G. Xie and S.-P. Chen, *Chem.-Eur. J.*, 2017, **23**, 17775–17787.
- 5 P. Zhang, L. Zhang, C. Wang, S.-F. Xue, S.-Y. Lin and J.-K. Tang, *J. Am. Chem. Soc.*, 2014, **136**, 4484–4487.
- 6 (a) S.-D. Jiang, B.-W. Wang, G. Su, Z.-M. Wang and S. Gao, *Angew. Chem., Int. Ed.*, 2010, **49**, 7448–7451; (b) N. F. Chilton, S. K. Langley, B. Moubaraki, A. Soncini, S. R. Batten and K. S. Murray, *Chem. Sci.*, 2013, **4**, 1719–1730; (c) T. T. da Cunha, J. Jung, M. E. Boulon, G. Campo, F. Pointillart, C. L. Pereira, B. Le Guennic, O. Cador, K. Bernot, F. Pineider, S. Golhen and L. Ouahab, *J. Am. Chem. Soc.*, 2013, **135**, 16332–16335; (d) F. Pointillart, K. Bernot, S. Golhen, B. Le Guennic, T. Guizouarn, L. Ouahab and O. Cador, *Angew. Chem., Int. Ed.*, 2015, **54**, 1504–1507; (e) Y. Bi, Y.-N. Guo, L. Zhao, Y. Guo, S.-Y. Lin, S.-D. Jiang, J. Tang, B.-W. Wang and S. Gao, *Chem. - Eur. J.*,



2011, **17**, 12476–12481; (f) J. Wu, O. Cador, X. L. Li, L. Zhao, B. Le Guennic and J. K. Tang, *Inorg. Chem.*, 2017, **56**, 11211–11219; (g) M. Guo, J.-F. Wu, O. Cador, J.-J. Lu, B. Yin, B. L. Guennic and J.-K. Tang, *Inorg. Chem.*, 2018, **57**, 4534–4542.

7 (a) K. R. Meihaus and J. R. Long, *J. Am. Chem. Soc.*, 2013, **135**, 17952–17957; (b) L. Ungur, J. J. Le Roy, I. Korobkov, M. Murugesu and L. F. Chibotaru, *Angew. Chem., Int. Ed.*, 2014, **53**, 4413–4417; (c) K. L. Harriman and M. Murugesu, *Acc. Chem. Res.*, 2016, **49**, 1158–1167; (d) F. Gendron, B. Pritchard, H. Bolvin and J. Autschbach, *Dalton Trans.*, 2015, **44**, 19886–19900.

8 (a) Y.-S. Ding, N. F. Chilton, R. E. P. Winpenny and Y.-Z. Zheng, *Angew. Chem., Int. Ed.*, 2016, **55**, 16071–16074; (b) J.-L. Liu, Y.-C. Chen, Y.-Z. Zheng, W.-Q. Lin, L. Ungur, W. Wernsdorfer, L. F. Chibotaru and M.-L. Tong, *Chem. Sci.*, 2013, **4**, 3310–3316; (c) S. K. Gupta, T. Rajeshkumar, G. Rajaraman and R. Murugavel, *Chem. Sci.*, 2016, **7**, 5181–5191; (d) Y.-C. Chen, J.-L. Liu, Y. Lan, Z.-Q. Zhong, A. Mansikkam-ki, L. Ungur, Q.-W. Li, J.-H. Jia, L. F. Chibotaru, J.-B. Han, W. Wernsdorfer, X.-M. Chen and M.-L. Tong, *Chem. - Eur. J.*, 2017, **23**, 5708–5715.

9 N. F. Chilton, C. A. Goodwin, D. P. Mills and R. E. Winpenny, *Chem. Commun.*, 2015, **51**, 101–103.

10 (a) W.-B. Sun, P.-F. Yan, S.-D. Jiang, B.-W. Wang, Y.-Q. Zhang, H.-F. Li, P. Chen, Z.-M. Wang and S. Gao, *Chem. Sci.*, 2016, **7**, 684–691; (b) P.-P. Cen, S. Zhang, X.-Y. Liu, W.-M. Song, Y.-Q. Zhang, G. Xie and S.-P. Chen, *Inorg. Chem.*, 2017, **56**, 3644–3656.

11 G.-J. Chen, C.-Y. Gao, J.-L. Tian, J.-K. Tang, W. Gu, X. Liu, S.-P. Yan, D.-Z. Liao and P. Cheng, *Dalton Trans.*, 2011, **40**, 5579–5583.

12 (a) S.-Y. Lin, Y.-N. Guo, Y. Guo, L. Zhao, P. Zhang, H.-S. Ke and J.-K. Tang, *Chem. Commun.*, 2012, **48**, 6924–6926; (b) X.-L. Li, H. Li, D.-M. Chen, C. Wang, J. Wu, J.-K. Tang, W. Shi and P. Cheng, *Dalton Trans.*, 2015, **44**, 20316–20320; (c) L. Zhang, P. Zhang, L. Zhao, J.-F. Wu, M. Guo and J.-K. Tang, *Inorg. Chem.*, 2015, **54**, 5571–5578.

13 (a) W. B. Sun, B. Yan, L.-H. Jia, B.-W. Wang, Q. Yang, X. Cheng, H.-F. Li, P. Chen, Z.-M. Wang and S. Gao, *Dalton Trans.*, 2016, **45**, 8790–8794; (b) S. Zhang, H.-S. Ke, L. Sun, X. Li, Q. Shi, G. Xie, Q. Wei, D.-S. Yang, W.-Y. Wang and S.-P. Chen, *Inorg. Chem.*, 2016, **55**, 3865–3871; (c) X.-J. Zhang, V. Vieru, X.-W. Feng, J.-L. Liu, Z.-J. Zhang, B. Na, W. Shi, B.-W. Wang, A. K. Powell, L. F. Chibotaru, S. Gao, P. Cheng and J. R. Long, *Angew. Chem., Int. Ed.*, 2015, **54**, 9861–9865.

14 Y.-N. Guo, X.-H. Chen, S. F. Xue and J.-K. Tang, *Inorg. Chem.*, 2011, **50**, 9705–9713.

15 (a) M. Gregson, N. F. Chilton, A. M. Ariciu, F. Tuna, I. F. Crowe, W. Lewis, A. J. Blake, D. Collison, E. J. L. McInnes, R. E. P. Winpenny and S. T. Liddle, *Chem. Sci.*, 2016, **7**, 155–165; (b) K. S. Lim, J. J. Baldoví, W. R. Lee, J. H. Song, S. W. Yoon, B. J. Suh, E. Coronado, A. Gaita-Arinò and C. S. Hong, *Inorg. Chem.*, 2016, **55**, 5398–5404; (c) J.-F. Wu, J.-L. Jung, P. Zhang, H.-X. Zhang, J.-K. Tang and B. Le Guennic, *Chem. Sci.*, 2016, **7**, 3632–3639.

16 (a) G.-J. Chen, Y.-N. Guo, J.-L. Tian, J.-K. Tang, W. Gu, X. Liu, S.-P. Yan, P. Cheng and D.-Z. Liao, *Chem.-Eur. J.*, 2012, **18**, 2484–2487; (b) F. Habib, G. Brunet, V. Vieru, I. Korobkov, L. F. Chibotaru and M. Murugesu, *J. Am. Chem. Soc.*, 2013, **135**, 13242–13245; (c) J. Zhu, C.-Z. Wang, F. Luan, T.-Q. Liu, P.-F. Yan and G.-M. Li, *Inorg. Chem.*, 2014, **53**, 8895–8910; (d) T. Pugh, F. Tuna, L. Ungur, D. Collison, E. J. McInnes, L. F. Chibotaru and R. A. Layfield, *Nat. Commun.*, 2015, **6**, 7492; (e) W. Cao, C. Gao, Y. Q. Zhang, D. Qi, T. Liu, K. Wang, C. Duan, S. Gao and J. Z. Jiang, *Chem. Sci.*, 2015, **6**, 5947–5954; (f) T. Pugh, V. Vieru, L. F. Chibotaru and R. Layfield, *Chem. Sci.*, 2016, **7**, 2128–2137.

17 L. Krause, R. Herbst-Irmer, G. M. Sheldrick and D. Stalke, *J. Appl. Crystallogr.*, 2015, **48**, 3–10.

18 G. M. Sheldrick, *Acta Crystallogr.*, 2008, **A64**, 112–122.

19 J. Luzon and R. Sessoli, *Dalton Trans.*, 2012, **41**, 13556–13567.

20 B. O. Roos, P. R. Taylor and P. E. M. Siegbahn, *Chem. Phys.*, 1980, **48**, 157–173.

21 F. Aquilante, L. De Vico, N. Ferre, G. Ghigo, P. A. Malmqvist, P. Neogrady, T. B. Pedersen, M. Pitonak, M. Reiher, B. O. Roos, L. Serrano-Andres, M. Urban, V. Veryazov and R. Lindh, *J. Comput. Chem.*, 2010, **31**, 224–247.

22 F. Aquilante, J. Autschbach, R. K. Carlson, L. F. Chibotaru, M. G. Delcey, L. De Vico, I. F. Galvan, N. Ferre, L. M. Frutos, L. Gagliardi, M. Garavelli, A. Giussani, C. E. Hoyer, G. Li Manni, H. Lischka, D. Ma, P. A. Malmqvist, T. Muller, A. Nenov, M. Olivucci, T. B. Pedersen, D. Peng, F. Plasser, B. Pritchard, M. Reiher, I. Rivalta, I. Schapiro, J. Segarra-Martí, M. Stenrup, D. G. Truhlar, L. Ungur, A. Valentini, S. Vancoillie, V. Veryazov, V. P. Vysotskiy, O. Weingart, F. Zapata and R. Lindh, *J. Comput. Chem.*, 2016, **37**, 506–541.

23 P. Malmqvist, B. O. Roos and B. Schimmelpfennig, *Chem. Phys. Lett.*, 2002, **357**, 230–240.

24 B. A. Hess, C. M. Marian, U. Wahlgren and O. Gropen, *Chem. Phys. Lett.*, 1996, **251**, 365–371.

25 B. O. Roos, R. Lindh, P. Malmqvist, V. Veryazov and P. Widmark, *J. Phys. Chem. A*, 2004, **108**, 2851–2858.

26 B. O. Roos, R. Lindh, P. Malmqvist, V. Veryazov and P. Widmark, *J. Phys. Chem. A*, 2005, **109**, 6575–6579.

27 B. O. Roos, R. Lindh, P. Malmqvist, V. Veryazov, P. Widmark and A. C. Borin, *J. Phys. Chem. A*, 2008, **112**, 11431–11435.

28 L. F. Chibotaru and L. Ungur, *J. Chem. Phys.*, 2012, **137**, 064112.

29 L. F. Chibotaru, *Adv. Chem. Phys.*, 2013, **153**, 397–519.

30 M. Llunell, D. Casanova, J. Cirera, P. Alemany and S. Alvarez, *SHAPE*, Universitat de Barcelona, Barcelona, 2013, vol. 2.1.

31 S. Zhang, H. P. Wu, L. Sun, H. S. Ke, S. P. Chen, B. Yin, Q. Wei, D. S. Yang and S. L. Gao, *J. Mater. Chem. C*, 2017, **5**, 1369–1382.

32 (a) H. S. Ke, S. Zhang, X. Li, Q. Wei, G. Xie, W.-Y. Wang and S.-P. Chen, *Dalton Trans.*, 2015, **44**, 21025–21031; (b) L. Zhang, P. Zhang, L. Zhao, S.-Y. Lin, S.-F. Xue, J.-K. Tang and Z.-L. Liu, *Eur. J. Inorg. Chem.*, 2013, **2013**, 1351–1357; (c) B. Joarder, A. K. Chaudhari, G. Rogez and S. K. Ghosh,

*Dalton Trans.*, 2012, **41**, 7695–7699; (d) L. Liang, G. Peng, G.-Z. Li, Y.-H. Lan, A. K. Powell and H. Deng, *Dalton Trans.*, 2012, **41**, 5816–5823.

33 S. Osa, T. Kido, N. Matsumoto, N. Re, A. Pochaba and J. Mroziniski, *J. Am. Chem. Soc.*, 2004, **126**, 420–421.

34 (a) A. Yamashita, A. Watanabe, S. Akine, T. Nabeshima, M. Nakano, T. Yamamura and T. Kajiwara, *Angew. Chem., Int. Ed.*, 2011, **123**, 4102–4105; (b) H. L. C. Feltham, Y. Lan, F. Klöwer, L. Ungur, L. F. Chibotaru, A. K. Powell and S. Brooker, *Chem.-Eur. J.*, 2011, **17**, 4362–4365; (c) S.-D. Jiang, B.-W. Wang, H.-L. Sun, Z.-M. Wang and S. Gao, *J. Am. Chem. Soc.*, 2011, **133**, 4730–4733.

35 (a) X. C. Huang, M. Zhang, D. Y. Wu, D. Shao, X.-H. Zhao, W. Huang and X.-Y. Wang, *Dalton Trans.*, 2015, **44**, 20834–20838; (b) Y.-Z. Tong, C. Gao, Q.-L. Wang, B.-W. Wang, S. Gao, P. Cheng and D.-Z. Liao, *Dalton Trans.*, 2015, **44**, 9020–9026.

36 (a) L. Sorace, C. Benelli and D. Gatteschi, *Chem. Soc. Rev.*, 2011, **40**, 3092–3104; (b) L. Ungur, S.-Y. Lin, J.-K. Tang and L. F. Chibotaru, *Chem. Soc. Rev.*, 2014, **43**, 6894–6905.

37 L. F. Chibotaru, *Struct. Bonding*, 2015, **164**, 185–230.

38 L. Ungur and L. F. Chibotaru, *Inorg. Chem.*, 2016, **55**, 10043–10056.

39 M. Li, H. P. Wu, Q. Yang, H.-S. Ke, B. Yin, Q. Shi, W.-Y. Wang, Q. Wei, G. Xie and S. P. Chen, *Chem.-Eur. J.*, 2017, **23**, 17775–17787.

40 L. Ungur and L. F. Chibotaru, *Phys. Chem. Chem. Phys.*, 2011, **13**, 20086–20090.

41 L. Ungur and L. F. Chibotaru, Computational Modelling of the Magnetic Properties of Lanthanide Compounds. in, *Lanthanides and Actinides in Molecular Magnetism*, ed. R. A. Layfield and M. Murugesu, Wiley-VCH Verlag GmbH & Co. KGaA, 1st edn, 2015, chp. 6, pp. 153–184.

42 D. Aravena and E. Ruiz, *Inorg. Chem.*, 2013, **52**, 13770–13778.

43 Z. J. Jiang, L. Sun, Q. Yang, B. Yin, H. S. Ke, J. Han, Q. Wei, G. Xie and S. P. Chen, *J. Mater. Chem. C*, 2018, **6**, 4273–4280.

